nature geoscience

SUPPLEMENTARY INFORMATION

DOI: 10.1038/NGEO2886

In the format provided by the authors and unedited.

Iron-dependent nitrogen cycling in a ferruginous lake and the nutrient status of Proterozoic oceans

Céline C. Michiels, François Darchambeau, Fleur A. E. Roland, Cédric Morana, Marc Llirós, Tamara García-Armisen, Bo Thamdrup, Alberto V. Borges, Donald E. Canfield, Pierre Servais, Jean-Pierre Descy and Sean A. Crowe

S1. Fe-dependent NO_3^- reduction – thermodynamic considerations

In order to test the thermodynamic favourability of reactions involving the different possible intermediates in Fe-dependent NO_3^- reduction, we calculated the relevant Gibbs free energy yields (see table S1). *In situ* concentrations for the different chemical species implicated are depicted in table S2. Temperature considered was 297°K (i.e., 23.85ºC) and the gas constant (R) used was 0.008314 kJ K^{-1} mol^{-1}. Under Kabuno Bay conditions (table S2), all the reactions outlined in table S1 are thermodynamically favourable.

S2. Denitrification and DNRA rates summary in Kabuno Bay

Rates of DNRA and denitrification have been calculated by linear-regressions with the least squares method over the time interval during which data are linear (24 or 48hrs) for $^{15}NH_4^+$ or $^{30}N_2$ production, respectively. The rates and the error associated are displayed in table S3.

S3. Dark carbon fixation in Kabuno Bay

Recent literature described the carbon fixation efficiency of Fe(II) dependent NO_3^- reducers from coastal marine sediments as being 1 mole of CO_2 fixed per 26.5 moles of Fe oxidized (Laufer et al, 2016). The products of NO_3^- reduction were not fully known in this case but the authors hypothesized based on the reaction stoichiometry that it leads to N_2 production. Therefore, because 5 moles of Fe(II) are needed to reduce 1 mole of NO_3^-, the carbon fixation efficiency for denitrification would be 0.18 ($r_{C/Denitr}$). By applying a factor of 8/5 to $r_{C/Denitr}$, we hypothesize a ratio to DNRA ($r_{C/DNRA}$) of 0.3. These factors are similar to those described for

sulphide dependent NO_3^- reducers by Klatt and Polerecky, 2015. Indeed, ratios of CO_2 fixed per NO_3^- used through sulphide dependent denitrification (to N_2) vary from 0.13 to 0.36 (Klatt and Polerecky, 2015). By applying a factor of 8/5 to $r_{C/Denitri}$, we adapted the ratio to DNRA ($r_{C/DNRA}$), which then varies from 0.21 to 0.58. In practice, growth yields for DNRA may differ from denitrification, and this stands as an important opportunity for future research.

With 40% DNRA and 60% denitrification, the contribution of NO_3^- reduction to total dark carbon fixation (Lliros et al. 2015) is 2 % (summarized in table S4) based on the ratio inferred from Laufer et al. 2016.

S4. Box-model of C, N, S and Fe cycling for a hypothetical Proterozoic upwelling system

The model used in the present study is based on the model developed by Canfield (2006) for a modern coastal upwelling system. It was previously adapted to a Proterozoic upwelling system by Boyle *et al.* 2013 showing that euxinia was only present when N_2-fixation occurred in the photic zone. The general structure of our 5 box model is briefly summarized in the main text, figure S1 as well as in figure 3a. We kept Canfield's (2006) model structure and dimensions (described in figure S1), as well as most model parameters (described in figure S1 and table S5), but added DNRA as well as the Fe-cycle to our model. N-fixation was not considered here as the model sustains export production without its contribution, and N-fixation is commonly absent in modern upwelling systems. Upwelling rates are represented with the coefficient A and B (cm hr^{-1}, see figure S1 and table S5) and vertical exchange between the different boxes is represented by the different K coefficients (cm hr^{-1}, see figure S1 and table S5).

Upwelled waters bring nutrients to the euphotic zone (here NO_3^- and/or NH_4^+), setting rates of primary production are based on N limitation. Primary production, also called export production in Boyle *et al*. 2013 is described as follows (equation 1):

$$EP = EP_{NO3-} + EP_{NH4+} = \frac{(A+B+K_u)}{r_{N:C}} (NO_{3\,um} + NH_{4\,um}) \quad (1)$$

Primary production is exported through sedimentation to the intermediate box (UM), where microbial respiration occurs. In the UM box, part of sedimented organic matter is degraded through oxic respiration, which together with nitrification consumes oxygen. Nitrification, in

turn, produces NO_3^-. Oxic respiration ($R_{aerobic}$) is limited by the oxygen diffusing from the surface waters (U box) into the UM box. Surface water oxygen was set assuming equilibrium with the atmosphere, and oxygen concentrations based on the reconstructions from the geologic record. We can calculate the rate of $R_{aerobic}$, which includes nitrification, based on the flux of oxygen entering the UM box, as shown in equation 2.

(2) $$R_{aerobic} = \frac{K_u O_{2u} + (A + K_{um}) O_{2D} + (K_I + B) O_{2I}}{r_{O2:C}}$$

Considering that oxygen can only come from the U box, equation 2 simplifies as:

(3) $$R_{aerobic} = \frac{K_u O_{2u}}{r_{O2:C}}$$

All oxygen was consumed through combined respiration and nitrification directly in the UM box.

NO_3^- reduction proceeds first using Fe(II) as an electron donor. For low upwelling rates, NO_3^- limits Fe-dependent NO_3^- reduction, and we can therefore calculate rates of NO_3^- reduction based on the supply of NO_3^- to the UM box as follows:

(4) $$R_{NO3-Fe} = (A + K_{um}) NO3_D + (B + K_I) NO3_I + r_{N:C}\, R_{aerobic}$$

NO_3^- is supplied through upwelling from intermediate waters and is also produced through nitrification in the UM box. Eq. (4) implies that NO_3^- in the UM box is consumed entirely and is therefore zero. If Fe(II) is limiting (instead of NO_3^-), on the other hand, we can calculate rates of Fe-dependent NO_3^- reduction based on the supply of Fe(II) to the UM box instead of the supply of NO_3^-:

(5) $$R_{NO3-Fe} = \left((A + K_{um}) Fe_D + (B + K_I) Fe_I\right) * r_{NO3/Fe}$$

with $r_{NO3/Fe}$ defined in eq. 11 below.

In order to determine whether NO_3^- or Fe(II) is limiting, we compared the supply rates of both (eqs. (4) and (5)) and considered the lowest as the actual rate of Fe-dependent

NO_3^- reduction ($R_{NO3\text{-}Fe}$). If Fe(II) is limiting, there will be NO_3^- left in the UM box that then fuels organic matter oxidation. This yields both Fe and C-dependent NO_3^- reduction in the UM box. The NO_3^- allocated to C-dependent NO_3^- reduction ($R_{NO3\text{-}C}$) can be calculated by subtracting (4)-(5). Again, the NO_3^- concentration in the UM box is zero as it is all consumed through a combination of Fe and C-dependent NO_3^- reduction. In summary:

Case 1: NO_3^- limiting Fe-dependent NO_3^- reduction

(6) $R_{NO3\ tot} = R_{NO3\text{-}Fe}$

Case 2: Fe(II) limiting Fe-dependent NO_3^- reduction

(7) $R_{NO3\ tot} = R_{NO3\text{-}Fe} + R_{NO3\text{-}C}$

As mentioned here above, we considered both DNRA and denitrification as part of NO_3^- reduction. By doing so, we are able to evaluate the effect of the partitioning between DNRA and denitrification on primary production, sulphate reduction rates, and the accumulation of hydrogen sulphide. We therefore varied the relative contributions of DNRA and denitrification to overall NO_3^- reduction and this ultimately influences the loss of N from the system versus recycling to NH_4^+ through DNRA. In order to address this balance between the two pathways, we reformulated the description of NO_3^- reduced per molecule of electron donor consumed (Fe(II) or organic matter) so that it reflected the overall stoichiometry of combined DNRA and denitrification. Denitrification consumes 5 electrons per NO_3^- reduced versus the 8 electrons involved in DNRA. The half reactions for denitrification and DNRA are the following:

(8) Denitrification: $NO_3^- + 5\ e^- + 6\ H^+ \rightarrow \frac{1}{2}\ N_2 + 3\ H_2O$

(9) DNRA: $NO_3^- + 8\ e^- + 10\ H^+ \rightarrow NH_4^+ + 3\ H_2O$

For Fe-dependent NO_3^- reduction, we considered the following half reaction:

(10) $Fe^{2+} + 3\ H_2O \rightarrow Fe(OH)_3 + 1\ e^- + 3\ H^+$

With x being the contribution of DNRA to NO_3^- reduction and (1-x) the contribution of denitrification, we can define the number of moles of NO_3^- used per mole of Fe(II) in eq. (11).

(11) $$r_{NO3:Fe} = (\frac{x}{8} + \frac{(1-x)}{5})$$

We also can define the number of moles of NH_4^+ released per mole of Fe(II) in eq. (12).

(12) $$r_{NH4:Fe} = \frac{x}{8}$$

Considering now C-dependent NO_3^- reduction, the half reaction of organic C oxidation used here is:

(13) $C_{106}H_{175}N_{16}O_{42}P + 280\ H_2O \rightarrow 106\ HCO_3^- + 16\ NH_4^+ + HPO_4^{2-} + 564\ H^+ + 472\ e^-$

Eq. 14 shows the number of moles of NO_3^- consumed per mole of organic C with a varying contribution of DNRA and denitrification to NO_3^- reduction.

(14) $$r_{NO3:C} = \frac{472\ (\frac{x}{8} + \frac{(1-x)}{5})}{106}$$

Finally, eq. 15 was modified from Boyle *et al.* 2013, so that $r_{NH4:C}$, accounted for both NH_4^+ released from remineralization of organic matter through NO_3^- reduction as well as the production of NH_4^+ through DNRA per mole of C oxidized. $r_{NH4:C}$ is therefore written as follows:

(15) $$r_{NH4:C} = \frac{16+59\,y}{106}$$

As NO_3^- in the UM box equals 0, the eq. 1 for export production can therefore be simplified to:

(16) $$EP = \frac{(A+B+K_u)}{r_{N:C}}\ NH_{4\ um}$$

With $NH_4^+{}_{UM}$ calculated in eq. 17, taking into account the ammonium released from NO_3^- reduction through DNRA (both Fe and C-dependent), we can therefore calculate eq. (16).

(17) $$NH4_{um} = \frac{(A+K_{um})NH4_D+(B+K_I)NH4_I+ r_{NH4:Fe}\, R_{NO3-Fe}+r_{NH4:C}\, R_{NO3-C}-r_{N:C}\, R_{aerobic}}{(K_{um}+K_I)}$$

If organic matter remains after exhausting NO_3^- in the UM box, the remaining amount can be oxidized through iron and sulphate reduction. Iron reduction was insignificant, and wasn't considered further. Sulfate reduction rates can be written as:

(18) $$R_{SR} = EP - R_{aerobic} - \frac{R_{NO3-C}}{r_{NO3:C}}$$

The sulphide produced through R_{SR} in the UM box being described in Eq. (19):

(19) $$H_2S_{um} = \frac{59}{106}\ \frac{R_{SR}}{(A+B+K_I+K_{um}+K_u)}$$

With eq. (20) as the half reaction used for sulphate reduction

(20) $SO_4^{2-} + 8\ e^- + 10\ H^+ \rightarrow H_2S + 4\ H_2O$

Finally, based on the rate of highly reactive Fe entering the UM box and the rate of H_2S produced through sulphate reduction, we can then infer the ratio of Fe-pyrite to highly reactive Fe used in the rock record to distinguish euxinic from ferruginous conditions.

(21) $$r_{Fe\ PY/HR\ Fe} = \frac{\frac{R_{SR}*59}{106}}{2*((A+K_{um})Fe_D+(B+K_I)Fe_I)}$$

Supplemental conditions from figure 3 b and c are displayed here below in figure S2 for the Fe-pyrite to highly reactive Fe ratio under 2 atmospheric oxygen concentrations (3.8% and 6.2% PAL) and for higher contributions of DNRA to NO_3^- reduction. Results show that euxinic conditions are reached at upwelling rates lower than when the contribution of DNRA is smaller, and without the need of an increased ammonium supply from the deep ocean.

The main parameters are constrained in table S5. These are the benchmark values used for the runs of the model of the main text, if not stated otherwise in the text or legends of the figure. We provide further explanation on how specific parameters were constrained below.

In the main text, we explored the influence of oxygen on the model outputs from 0% to 12% PAL (figure 3d in the main text). 0% PAL is a special case where oxygen is not available locally for nitrification in the upwelling zone. However, we maintained the supply of NO_3^- from intermediate waters, as non-local oxygen oases are plausible in the Archean ocean, even under an ostensibly anoxic atmosphere (Olson et al. 2013). Therefore, these oxygen oases could have enabled the local production of NO_3^- through nitrification in other parts of the Archean ocean and supplied the NO_3^- to intermediate waters as considered in our box model.

We also tested a broad range in deep ocean Fe(II) and NH_4^+ concentrations, as mentioned in the main text. Indeed, these parameters are poorly constrained in the literature and we therefore studied the influence of likely ranges on our model outputs. Fe(II) concentrations are commonly thought to be controlled by equilibrium with siderite ($FeCO_3$), which yields between 40 to 120µM deep ocean Fe(II) (Holland, 1984). However, Derry 2015 suggests siderite formation was kinetically limited and Fe(II) concentrations may have been much higher (< 3mM). Assuming upwelled P is needed to fuel oxygenic photosynthesis and sustain appreciable atmospheric O_2 in the Proterozoic Eon, Fe(II) concentrations must then have been less than 424 times deep water P concentrations (Jones et al., 2015). Indeed, at Fe(II):P ratios greater than 424, upwelling P is consumed through photoferrotrophy and would therefore not reach the surface waters to support appreciable oxygenic photosynthesis. Based on these arguments, we chose an Fe(II) concentration 42µM (based on 424 x 0.1 µM P) for the benchmark in our model runs presented in the main text. However, we also tested a range of concentrations (from 10 to 500µM) that encompasses the values described by Holland 1984. We focused on the role of Fe(II) concentrations in dictating the Fe_{PY}/Fe_{HR} ratio across a suite of different model conditions in figure S3 (a-h). Overall, and as expected, without DNRA and at low deep ammonium concentrations (2µM, figure S3 a to d), ferruginous conditions tend to prevail as Fe(II) concentrations increase. However, with DNRA and at 10µM Fe(II) (figure S3 e), Fe(II) is limiting and euxinic conditions ($Fe_{PY}/Fe_{HR}>0.7$) develop at relatively low upwelling rates. Above 42µM on the other hand (figure S3 b-d, f-h), with or without DNRA, Fe(II) is supplied in excess and effectively titrates any sulphide produced through sulphate reduction,

invariably yielding ferruginous conditions (Fe_{PY}/Fe_{HR} <0.7). Figure S3 j to l depicts different concentrations of deep Fe(II) versus a wide range of deep NH_4^+ concentrations (between 0 and 15µM) without the contribution of DNRA (0% DNRA). This shows that euxinic conditions could also be reached without the contribution of DNRA, but mainly under low deep Fe(II) concentrations (between 10 and 42µM) and under relatively high NH_4^+ concentrations (>13µM), as mentioned in the main text.

Our benchmark model runs described in the main text invariably consider NO_3^- to be present in the intermediate waters. We then assumed that these intermediate waters would be Fe(II) free as it would have been consumed through NO_3^- reduction. The opposite could be true, on the other hand, and so we also tested this here to evaluate the effect of Fe(II) bearing NO_3^- free intermediate waters. When intermediate waters contain Fe(II), we added equimolar NH_4^- instead of NO_3^-, accordingly. Results of this test are depicted in figure S4 and show that, although export production is very high compared to the benchmark model scenarios, euxinic conditions (Fe_{PY}/Fe_{HR}>0.7) do not occur in the water column. Without a supply of NO_3^- through the intermediate waters, NO_3^- reduction is fuelled only through nitrification and therefore by the oxygen supply from the surface water (3.8% PAL in this test). This being minimal, NO_3^- reduction and N-loss are highly restricted.

S5. Global N-fixation and N-loss in the Archean and Proterozoic

Annual rates of marine N-fixation for the Proterozoic Eon are estimated based on the modern rates described in Gruber and Sarmiento 1997. In order to scale the modern rates to the Proterozoic Eon, we assumed that N-fixation was ultimately limited by P supply (Tyrrell, 1999) and was therefore proportional to deep ocean P concentrations. We thus divided the modern rates of 135 ± 50 Tg N yr^{-1} (encompassing both pelagic and benthic N-fixation) by the modern phosphorous concentration (2.3µM, Bjerrum and Canfield, 2002) in the deep ocean and multiplied this by the highest estimates for the phosphorous concentration (0.13µM) described for Paleoproterozoic oceans (Jones et al. 2015). The 4.8 Tg N yr^{-1} we report in the main text is our lowest estimate if we consider the error on the N-fixation estimate. To assess the extent to which we could apply the 0.13 µM deep water P concentration from Jones et al. (2015) across the Proterozoic Eon we took values of Fe/Si from the Rapitan iron-formation (Klein 2005) and applied these to Jones et al. 2015 model to infer phosphorous concentrations for the

Neoproterozoic oceans. Values found for the Rapitan were within the range of those calculated by Jones et al. 2015. We also considered trace metal limitation of N-fixation very unlikely. The most likely metal to limit N-fixation in the Proterozoic is molybdenum (Anbar and Knoll 2002). However, Helz et al. 1996 showed that high levels of sulphide (between 50 and 250µM) are necessary to effectively strip Mo from seawater under euxinia. Our model implies that under most reasonable scenarios sulphide concentrations do not exceed about 20µM and are therefore insufficient to trigger effective Mo removal.

Conservative rates of global N-loss were inferred from our box-model when denitrification contributes 100% of NO_3^- reduction (no DNRA, therefore higher N-loss) under 6.2% PAL, low ammonium conditions (2µM) and deep ocean Fe(II) concentrations of 42µM. The highest rates of N-loss were found with the highest upwelling rate explored in this model (3 cm hr^{-1}). We then extrapolated N-loss from our model to an area equivalent to upwelling regions in the modern ocean (0.36 10^{12} m^2) as indicated in the main text. In comparison, rates of N-loss under the lowest upwelling rate considered in our model (0.5 cm hr^{-1}) are 4 times lower than with an upwelling rate of 3 cm hr^{-1}.

Table S1: Free Gibbs Energy yield in standard conditions (ΔG˚) and for Kabuno Bay concentrations (ΔG). Values for ΔG˚ can be found in Canfield, Kristensen and Thamdrup 2005

Reactions	ΔG˚ (kJ /mol N)	ΔG (kJ /mol N)
$8\ Fe^{2+} + 21\ H_2O + \mathbf{NO_3^-} \Rightarrow \mathbf{NH_4^+} + 8\ Fe(OH)_3 + 14\ H^+$	51.67	-272.41
$5\ Fe^{2+} + 12\ H_2O + \mathbf{NO_3^-} \Rightarrow 0.5\ \mathbf{N_2} + 5\ Fe(OH)_3 + 9\ H^+$	-143.19	-336.97
$6\ Fe^{2+} + 16\ H_2O + \mathbf{NO_2^-} \Rightarrow \mathbf{NH_4^+} + 6\ Fe(OH)_3 + 10\ H^+$	31.93	-189.81
$3\ Fe^{2+} + 7\ H_2O + \mathbf{NO_2^-} \Rightarrow 0.5\ \mathbf{N_2} + 3\ Fe(OH)_3 + 7\ H^+$	-162.93	-328.28
$2\ Fe^{2+} + 4.5\ H_2O + \mathbf{NO_2^-} \Rightarrow 0.5\ \mathbf{N_2O} + 2\ Fe(OH)_3 + 3\ H^+$	-83.85	-137.86
$4\ Fe^{2+} + 11.5\ H_2O + 0.5\ \mathbf{N_2O} \Rightarrow \mathbf{NH_4^+} + 4\ Fe(OH)_3 + 7\ H^+$	115.78	-51.95
$Fe^{2+} + 2.5\ H_2O + 0.5\ \mathbf{N_2O} \Rightarrow 0.5\ \mathbf{N_2} + Fe(OH)_3 + 2\ H^+$	-158.16	-186.59
$2\ Fe^{2+} + 5\ H_2O + \mathbf{NO_3^-} \Rightarrow \mathbf{NO_2^-} + 2\ Fe(OH)_3 + 4\ H^+$	19.74	-82.60

Table S2: Chemical species concentrations (in μM) representative for the chemocline in Kabuno Bay

Chemical species	Concentration (μM)
NO_3^-	1
NO_2^-	1
N_2O	0.01
NH_4^+	100
Fe (II)	100
$Fe(OH)_3$	10^6 activity=1 as a pure solid
pH	6.5

Table S3: Summary of DNRA and denitrification rates for KB's water column. Rates were calculated over 48 hours unless stated otherwise next to the calculated rates.

Depth (m)	$^{30}N_2$ production (nmol N d^{-1})	$^{30}N_2$ production (nmol N d^{-1}) with Fe added	$^{15}NH_4^+$ production (nmol N d^{-1})	$^{15}NH_4^+$ production (nmol N d^{-1}) with Fe added
9.5	0 ± 0	0 ± 0	0 ± 0	0 ± 0
10	0 ± 0	0 ± 0	0 ± 0	0 ± 0
10.5	0 ± 0	0 ± 0	0 ± 0	0 ± 0
11	80 ± 10	230 ± 40	20 ± 0 (24h)	70 ± 20 (24h)
11.5	50 ± 10	140± 20	50 ± 10 (24h)	70 ± 10

Table S4: Rates and ratio considered for calculations

Microbial process	Process rate measurements	Reference
Dark Carbon fixation	1.49µmol C L^{-1} d^{-1}	Lliros et al. 2015
DNRA	70 nmol N L^{-1} d^{-1}	This paper
Denitrification	230 nmol N L^{-1} d^{-1}	This paper

Table S5: Description of the different parameters used in the current model

Parameters	Value/ Units	Description	Reference
K_{um}	0.2 cm h^{-1}	Vertical exchange	Canfield 2006
K_u	0.1 cm h^{-1}	Vertical exchange	Canfield 2006
K_i	0.4 cm h^{-1}	Vertical exchange	Canfield 2006
A	0 cm h^{-1}	Upwelling Rate	Canfield 2006
B	0.5-3 cm h^{-1}	Upwelling Rate	Canfield 2006
O_{2u}	9.5-15.5 µM (3.8% to 6.2% PAL)	O_2 concentration in U box	Zhang *et al*. 2016
O_{2D}	0 µM	O_2 concentration in D box	Boyle *et al.* 2013
O_{2I}	0 µM	O_2 concentration in I box	Boyle *et al.* 2013
$r_{O2:C}$	170/117	Ratio of molecule of O_2 consumed for 1 molecule of carbon oxidized	Boyle *et al.* 2013
$r_{N:C}$	16/106	Ratio based on Redfield ratio	Redfield, 1934
EP	nmol C cm^{-2} h^{-1}	Rate of export production	
$R_{aerobic}$	nmol C cm^{-2} h^{-1}	Rate of aerobic respiration	
$R_{NO3\text{-}tot}$	nmol N cm^{-2} h^{-1}	Rate of nitrate reduction through Fe dependent nitrate reduction (if case 1) or through Fe and C dependent NO_3^- reduction (if case 2)	
$R_{NO3\text{-}Fe}$	nmol N cm^{-2} h^{-1}	Rate of nitrate reduction through Fe dependent NO_3^- reduction	
$R_{NO3\text{-}C}$	nmol N cm^{-2} h^{-1}	Rate of nitrate reduction through C dependent NO_3^- reduction (only case 2)	
R_{SR}	nmol C cm^{-2} h^{-1}	Rate of sulphate reduction	
$R_{Fe\text{-}ox}$	nmol Fe cm^{-2} h^{-1}	Rate of Fe oxidation	
$NH4_{UM}$, $NH4_D$, $NH4_I$	TBD, 2, 0 µM	Ammonium concentration in UM, D, I box	Deep water concentrations based on Jones et al. 2015 Phosphorous concentration estimates.
$NO3_{UM}$, $NO3_D$, $NO3_I$	TBD, 0, 1 µM	Nitrate concentration in UM, D, I box	Deep water concentrations based on Jones et al. 2015 Phosphorous concentration estimates.
Fe_{UM}, Fe_D, Fe_I	TBD, 42, 0 µM	Iron (II) concentration in UM, D, I box	Deep water concentrations based on Jones et al. 2015 Phosphorous concentration estimates.
H_2S_{UM}	TBD µM	Sulfide concentration in UM box	

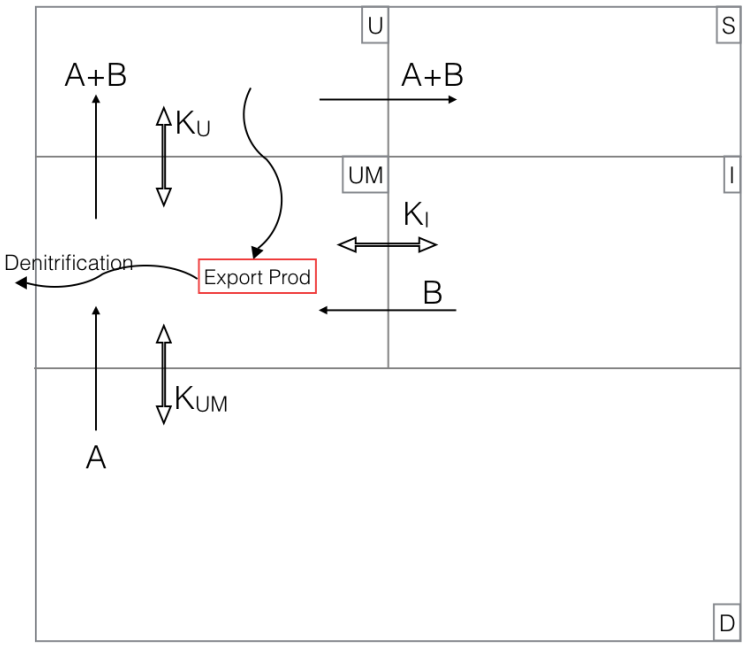

Figure S1: Box-model for C, N, S and Fe cycling in hypothetical Precambrian upwelling system adapted from Canfield (2006). Notation is as follows: Upwelling coefficients (A+B) from intermediate and deep waters (boxes I and D) as well as horizontal (K_I) and vertical mixing (K_u and K_{um}) between the UM box and the other boxes considered (I, U and D respectively). Box S represents ocean surface waters away from the upwelling zone. The parameter values are listed in table S5. Organic matter produced in the euphotic zone (box U) as export production settles to box UM where it is partially (in Canfield 2006) or entirely (Boyle et al. 2013 and this paper) degraded. The order of the pathways through which it is degraded is oxic respiration, followed by nitrate reduction (Canfield 2006 and Boyle *et al.* 2013), and finally by sulphate reduction.

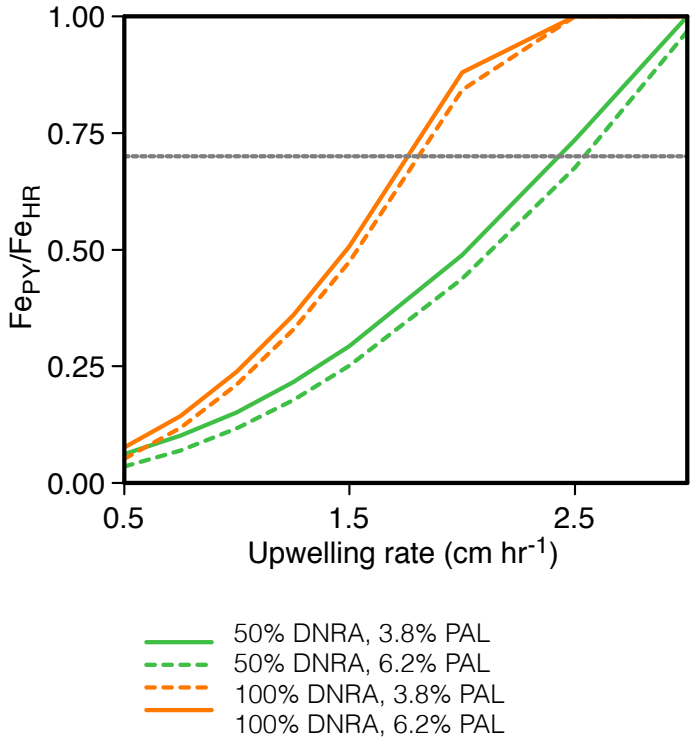

Figure S2: Fe-pyrite to highly reactive Fe ratio for 50 and 100% DNRA (in green and orange respectively) with varying surface waters oxygen (3.8% PAL in solid lines and 6.2%PAL in dashed lines) and for different upwelling rates. These model runs are for deep NH_4^+ concentrations of 2µM.

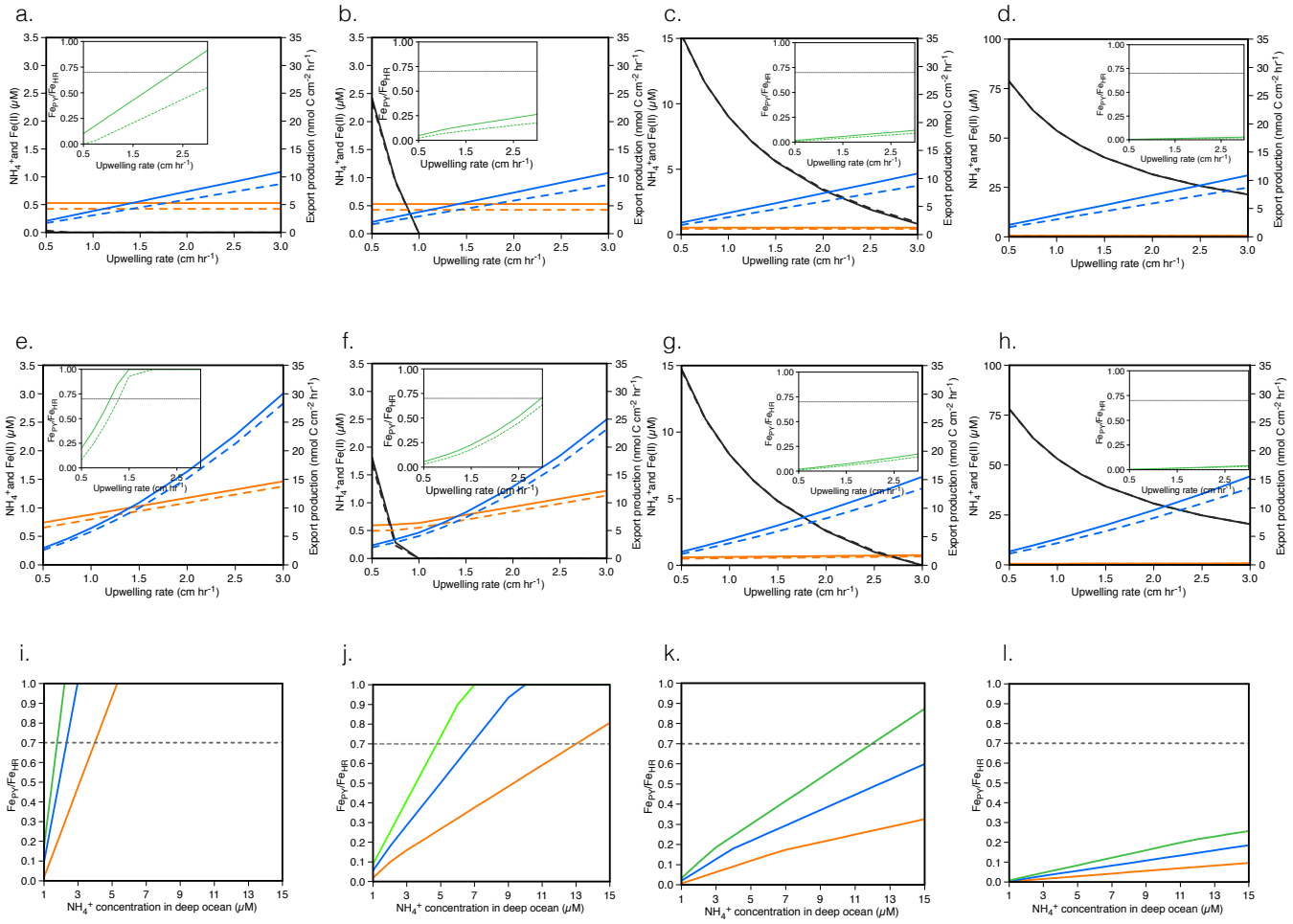

Figure S3: Graphs (a-d) represents model runs with 0% DNRA; (e-h) represents model runs with 30% DNRA. Solid lines represent model runs with the surface water oxygen concentrations of 3.8% PAL, whereas dashed lines represent runs at 6.2% PAL [blue=export production, orange= NH_4^+ concentrations, and black=Fe(II) concentrations, insets show the Fe-pyrite to highly reactive Fe ratio (Fe_{PY}/Fe_{HR}) where the grey line delineates plausible euxinic conditions]; (i-l) represent model runs of Fe_{PY}/Fe_{HR} ratios for a range of deep ocean NH_4^+ concentrations at 0% DNRA with surface water oxygen concentrations of 3.8% PAL (orange=upwelling rate of 1cm hr^{-1}, blue=upwelling rate of 2cm hr^{-1}, and green=upwelling rate of 3cm hr^{-1}). The first column of these graphs are for deep Fe(II) concentrations of 10μM, the second column is 42μM (as represented in the main text), the third is 120μM and the fourth is 500μM.

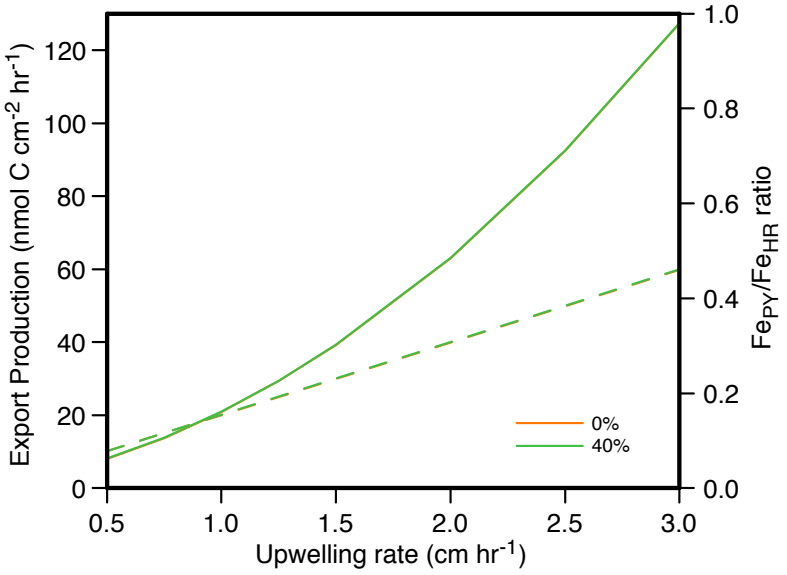

Figure S4: Run of the model with 20µM Fe(II) in the intermediate box (I) but no NO_3^-. Instead, upwelled waters from box I are bringing 1µM of NH_4^+ to the upwelled zone. Deep waters are bringing 42µM Fe(II) and 2µM NH_4^+. Solid lines represent export production whereas dashed lines represent Fe_{PY}/Fe_{HR} ratio. Case with 0% DNRA is in orange and case with 40%DNRA is in green, however, as the two cases yield very similar results, the orange case is hidden by the green.

Supplementary references

1 Canfield, D. E., Kristensen, E. & Thamdrup, B. Aquatic geomicrobiology. *Adv Mar Biol* **48**, 1-599, doi:10.1016/S0065-2881(05)48017-7 (2005).

2 Klatt, J. M. & Polerecky, L. Assessment of the stoichiometry and efficiency of CO2 fixation coupled to reduced sulfur oxidation. *Front Microbiol* **6**, 484, doi:10.3389/fmicb.2015.00484 (2015).

3 Lliros, M. *et al.* Pelagic photoferrotrophy and iron cycling in a modern ferruginous basin. *Sci Rep* **5**, 13803, doi:10.1038/srep13803 (2015).

4 Canfield, D. E. Models of oxic respiration, denitrification and sulfate reduction in zones of coastal upwelling. *Geochim Cosmochim Ac* **70**, 5753-5765, doi:Doi 10.1016/J.Gca.2006.07.023 (2006).

5 Boyle, R. A. *et al.* Nitrogen cycle feedbacks as a control on euxinia in the mid-Proterozoic ocean. *Nat Commun* **4**, doi:Artn 1533
Doi 10.1038/Ncomms2511 (2013).

6 Zhang, S. *et al.* Sufficient oxygen for animal respiration 1,400 million years ago. *Proc Natl Acad Sci U S A* **113**, 1731-1736, doi:10.1073/pnas.1523449113 (2016).

7 Redfield, A. C. The biological control of chemical factors in the environment. *Am Sci* **46**, 230A-221 (1958).

8 Jones, C., Nomosatryo, S., Crowe, S. A., Bjerrum, C. J. & Canfield, D. E. Iron oxides, divalent cations, silica, and the early earth phosphorus crisis. *Geology* **43**, 135-138, doi:10.1130/G36044.1 (2015).

9 Olson, S. L., Kump, L. R. & Kasting, J. F. Quantifying the areal extent and dissolved oxygen concentrations of Archean oxygen oases. *Chemical Geology* **362**, 35-43, (2013).

10 Holland, H. D. *The Chemical Evolution of the Atmosphere and Oceans*. (Princeton University Press, 1984).

11 Derry, L. A. Causes and consequences of mid-Proterozoic anoxia. *Geophys Res Lett* **42**, 8538-8546, doi:10.1002/2015gl065333 (2015).

12 Gruber, N. & Sarmiento, J. L. Global patterns of marine nitrogen fixation and denitrification. *Global Biogeochem Cy* **11**, 235-266, doi:Doi 10.1029/97gb00077 (1997).

13 Klein, C. Some Precambrian banded iron-formations (BIFs) from around the world: Their age, geologic setting, mineralogy, metamorphism, geochemistry, and origin. *Am Mineral* **90**, 1473-1499, doi:10.2138/am.2005.1871 (2005).

14 Tyrrell, T. The relative influences of nitrogen and phosphorus on oceanic primary production. *Nature* **400**, 525-531 (1999)

15 Bjerrum, C. J. & Canfield, D. E. Ocean productivity before about 1.9 Gyr ago limited by phosphorus adsorption onto iron oxides. *Nature* **417**, 159-162, doi:10.1038/417159a (2002).

16 Anbar, A. D. & Knoll, A. H. Proterozoic ocean chemistry and evolution: A bioinorganic bridge? *Science* **297**, 1137-1142, doi:DOI 10.1126/science.1069651 (2002).

17 Helz, G. R. *et al.* Mechanism of molybdenum removal from the sea and its concentration in black shales: EXAFS evidence. *Geochim Cosmochim Ac* **60**, 3631-3642, doi:Doi 10.1016/0016-7037(96)00195-0 (1996).